J Mater Sci: Mater Electron (2017) 28:5415–5424
DOI 10.1007/s10854-016-6202-x

Interface conduction and photo-induced electrical transport in the heterojunction formed by GaAs and Ce^{3+}-doped SnO_2

Diego H. O. Machado[1] · Luis V. A. Scalvi[1] · Américo Tabata[1] · José H. D. da Silva[1]

Received: 1 September 2016 / Accepted: 7 December 2016 / Published online: 17 December 2016

Abstract Electrical and optical properties of heterojunction composed of GaAs and SnO_2 are presented. SnO_2 thin film was deposited by sol-gel-dip-coating and doped with Ce^{3+} whereas the GaAs layer was deposited by resistive evaporation or sputtering. The purpose of this investigation is to combine the blue emission properties of the rare-earth with the unique transport properties generated by the heterojunction assembly. We have found that illumination with light of energy above the GaAs bandgap and below the SnO_2 bandgap decrease drastically the GaAs/SnO_2 heterojunction resistance. Under this condition, the sample exhibits an unusual behavior: the conductivity is practically temperature independent. This behavior was related with the presence of interface conduction, which could be associated to a two-dimensional electron gas at the GaAs/SnO_2 interface. This feature takes places only for the sample where the GaAs bottom layer is deposited by sputtering, which presents a smoother surface as inferred by AFM images. The deposition sequence of the layers is fundamental to provide sample excitation which strongly contributes to the sample conductivity. Energies above the SnO_2 bandgap only excite the top oxide layer. When the GaAs is the top layer it acts as a shield, and only effects from the ions located close to the interface SnO_2/GaAs are observed. Luminescence from the Ce^{3+} ion can be detected, but overlap with emission from the matrix. Results suggest that a more organized GaAs bottom layer may contribute for a more efficient emission and also for signal separation.

✉ Luis V. A. Scalvi
scalvi@fc.unesp.br

[1] Graduate Program in Materials Science and Technology, Department of Physics, FC and POSMAT, UNESP, São Paulo State University, Bauru, SP, Brazil

1 Introduction

The emission from rare-earths doped oxide semiconductors associated with the unique heterojunctions transport properties seems to be very promising for the assembly of optoelectronic devices. Oxide semiconductors, which generally present wide bandgap, can be doped with rare-earth ions, which reduce the thermal quenching effects [1], giving rise to high efficiency light emission. Tin dioxide (SnO_2) is a wide bandgap semiconductor (energy about 3.6 eV [2]) with more than 90% transparency in the visible range [2, 3]. However, luminescence from thin films is not as efficient as from xerogels. Sol–gel deposited thin films are composed of nanoscopic crystallites, which influence the emission spectra, due to the particle size [4]. The main difficulty of getting efficient light emission from thin films is probably related to the sample dimensions, where the number of emission centers in the excitation source path is small. There are a few publications reporting luminescence on rare-earth-doped SnO_2 films. On the other hand, gallium arsenide (GaAs) is one of the most essential semiconductors for microelectronics, used in applications where the interaction of light and electricity is required [5]. Its utility is mainly related to the direct bandgap transition, leading the excited electrons to occupy preferentially the higher mobility Γ valley of the conduction band [6].

SnO_2/GaAs heterojunctions thin films have been successfully obtained, giving birth to smooth interface and improved electrical properties [7, 8]. Photoluminescence (PL) from this sort of heterojunction where SnO_2 films is doped with Eu^{3+}, leads to identification of the Eu^{3+} transitions, which does not happen for SnO_2:Eu thin films deposited directly on top of glass substrates, without the GaAs layer [9].

Heterojunctions using transparent oxides deposited on top of semiconductors have been presented recently. For instance, high-quality self-textured ZnO films has been grown on top of a GaAs substrate, forming a heterojunction with characteristic of rectifying diode, with blue-violet and infrared electroluminescence [10], suitable for optical fiber telecommunications applications. Heterojunction *n*-ZnO/p-GaAs, where the oxide is deposited by spin-coating on top of a p-GaAs substrate, have been proposed as a diode with ideality factor greater than the unity. The non-ideal behavior is related to nanocrystalline nature of ZnO film and surface states of the interfacial layer [11]. Promising devices for the development of solid-state lighting were achieved by *n*-ZnO/*n*-GaAs heterostructured light-emitting diodes [12]. Other combinations of semiconductor heterojunctions with SnO_2 have been successfully used such as with gallium selenide (GaSe) [13]. CdTe/SnO_2 heterojunction has been proposed for solar cells devices [14] since the properties of CdTe, one of the best candidates for solar energy conversion, can be modulated by coupling with other materials. The combination of SnO_2 with Al_2O_3 layer deposited by similar processes of the films deposition used in this paper, has led to a simple device with a potential combination for application as transparent transistors [15–17].

Concerning the doping with ion Ce^{3+}, it presents $^4f_1$ electronic configuration at the ground state and $^5d_1$ at excited state. Optical transitions between these states are electric dipole allowed transitions. Level 5d presents strong lattice interaction and the first dipole transition suffers a spectroscopic redshift when incorporated into a crystal, being shifted towards lower energy compared to the free ion [18]. Broad blue emission has been observed around 489 nm in a host matrix of zinc borosilicate glass [19], being attributed to the transition from 5d excited level (2D) to $^4f_1$ ground state ($^2F_{5/2}$) of Ce^{3+}. The radius and charge difference between the rare-earth ion and Sn^{4+} makes the ion incorporation into the SnO_2 lattice difficult, which leads to a low quantum efficiency in the luminescence process [20]. In order to avoid this problem, it is recommended the production of materials in nanoparticle form [20]. To reach this goal, the sol–gel process has been widely used [21, 22]. $Gd(PO_3)_3$ doped with 1%Ce^{3+} and 1%Yb^{3+} has shown emission at 328 nm for excitation with 291 nm, and potential application for the improvement of solar cell devices efficiency [23]. Phosphors for application in LEDs have been obtained for the system Ca_2SiO_4:Ln (Ln = Ce^{3+}, Eu^{2+}, Sm^{3+}). PL data exhibit a blue emission centered at 426 nm, attributed to Ce^{3+} ion, from the excited 5d state to the ground state 4f, independent on doping concentration [24]. These phosphors have potential application for LED close to the UV radiation range.

It is also important to mention that the interface between layers has an important role on the optical and electrical properties in the proposed heterojunction. In the 1970s the concept of heterostructures, related to the combination between different materials, has boosted semiconductor Physics, influencing far beyond this field, because they could have their optical and electrical properties rearranged by combination of these materials [6]. The deposition of heterostructures with smooth and atomic quality surfaces has become a possibility since the late 1960s when the growth of epitaxy layers became available. Figure 1 shows the band energy diagram before and after the metallurgical junction of GaAs and SnO_2. Figure 1 (top) shows the band energy diagram separately, with their respective bandgap and Fermi level position (shifted to the upper half in the case of SnO_2—since it is naturally n type, and the intrinsic Fermi level in the case of GaAs). The junction of these materials leads to a discontinuity on the profile of conduction and valence bands due to the equilibrium condition: equality in the Fermi level at both sides. The interface of the semiconductors has intrinsic states, and the Fermi level at the surface is different from the bulk, thereby producing the bending of the band diagram in the interface region [8, 25], as shown in Fig. 1 (bottom). This band bending may lead to a charge accumulation layer at the interface, which means a two-dimensional electron gas (2DEG). The electrons provided by the SnO_2 layer lodge next to the GaAs interface, resulting in the formation of a nonuniform electric field. This interfacial region contains a large concentration of electrons, where they remain confined, in the triangular shape quantum well with a gas carrier behavior, presenting high electron mobility [7]. This quantum well may present energy discrete levels below the conduction band bottom of one or both materials. The electron confinement in the quantum well changes the nature of the electrical movement, thereby changing the scattering mechanisms and affecting the transport properties. The quantization of charge near surface and interface layers was first demonstrated by Tsui [26], using subband energies measurements. Normally, only the quantum mechanical ground state in the triangular well is populated, but the excited levels can be filled with the application of an electric field.

A 2DEG has recently been found also at the interface between two insulating oxides $LaAlO_3$ and $SrTiO_3$ [27], attracting significant interest due to possible applications in all-oxide electronic devices. Wang et al. [28] employed first-principles calculations to investigate the system $KNbO_3/ATiO_3$ (001) (A = Sr, Pb, and Ba) heterostructures where perovskites ferroelectrics, $KNbO_3$, $PbTiO_3$, and $BaTiO_3$, are used as oxide constituents to create a 2DEG at the interface, also promising candidate for applications in all-oxide electronic devices, since it is possible to control the 2DEG properties by external stimulus.

Considering that the formation of a 2DEG is a possibility at the interface SnO_2/GaAs [29], the proposal of this

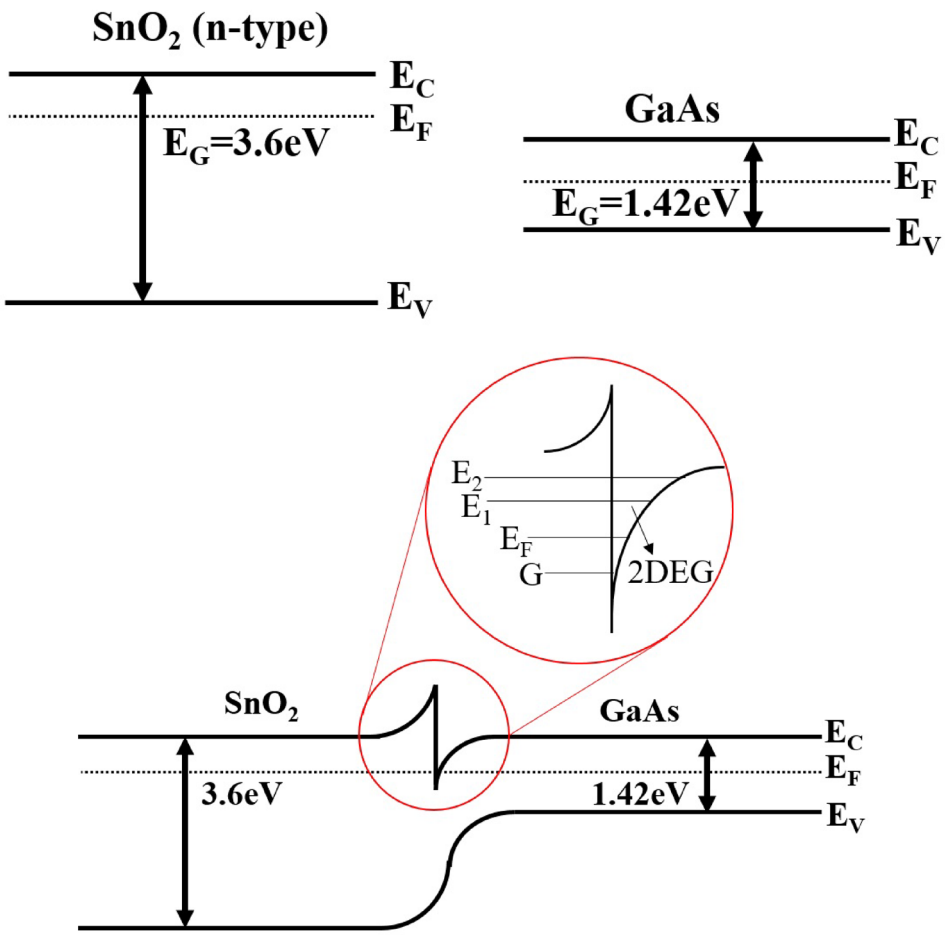

Fig. 1 *Top* Energy band diagram for semiconductors SnO_2 and GaAs (separated). *Bottom* when connected, after equilibrium condition is reached (Fermi level equality). *Inset* two-dimensional electron gas at the interface region. G is the ground state, E_1 and E_2 excited states

work is to combine the doping with trivalent Ce^{3+} ions in SnO_2 with a GaAs layer, originating a simple heterojunction SnO_2:Ce^{3+}/GaAs (or GaAs/SnO_2:Ce^{3+}). The electrical characteristic associated to the interface between both semiconductors indicates a very promising performance related to the electrical transport. The evaluation of conductivity as function of temperature data points to an unusual conductivity behavior. In order to understand the rule on the electrical transport, layers are also grown in opposite order, which means GaAs on top of SnO_2 and the temperature-dependent conductivity under monochromatic light excitation with distinct light sources is measured. Temperature dependent PL data are also shown, displaying the Ce^{3+} transitions and the potentiality for application of the heterojunction SnO_2/GaAs for optoelectronic devices.

2 Experimental

2.1 Synthesis of heterojunction

Colloidal suspension is produced by the sol–gel process, from solutions of $SnCl_4{\cdot}5H_2O$ and $Ce(NO_3)_3{\cdot}6H_2O$. Firstly, the 0.5 mol L^{-1} $SnCl_4{\cdot}5H_2O$ aqueous solution is prepared, followed by the addition of an appropriate amount of $Ce(NO_3)_3{\cdot}6H_2O$ in order to obtain the desired doping of Ce^{3+}, which is 1at% for all samples used in this work. Concentrated NH_4OH is added to the solution under stirring, until no more precipitation takes place (pH 11). This procedure provides a viscous and whitish solution, which is submitted to dialysis against distilled water for about 10 days for elimination of Cl^- and NH_4^+ ions. The resulting suspension presents a semitransparent aspect (sol). For the deposition of thin films, the sol is concentrated by elimination of about 70% of the initial volume and the films are deposited by the dip-coating technique on soda lime glass substrates with a withdrawal rate of 10 cm/min. Previous to deposition, the substrates, from Knittel Glaser, were kept in solution of 90% of deionized water and 10% of neutral detergent for 24h. Then it was cleaned in water followed by acetone, and dried with the help of a hot air flux drier. Layers are deposited at room temperature, gelling in air for 20 min and heated at 400 °C for 10 min in a furnace at room pressure. When the total of desired layers is reached, samples are submitted to thermal annealing, which generally is at 550 °C for 1 h in the same furnace. Resulting thickness of

films obtained by this procedure is about 300 nm [7]. The intermediate thermal treatment between layers is absent in the case where SnO_2 film is deposited on top of GaAs. In this case, the final annealing is for 150 °C by for 1h, procedure that does not damage the GaAs bottom layer.

GaAs films and In electrodes have been evaporated through the resistive evaporation technique. The soda lime glass substrates received a similar cleaning procedure as employed for SnO_2 deposition, as described above. The used GaAs source is from Sigma Aldrich, in small pieces, with purity 99.999%, and density 5.31 g/cm^3 at 25 °C. The pieces were smashed in order to become a fine particle powder, which helps the evaporation procedure under vacuum. Metallic In deposition is carried out to make electric contacts to the films, in order to accomplish electrical measurements. Figure 2 shows the sample geometry, displaying the as grown layers, and the In contact on top of it, along with the layout to perform electrical characterization measurements. These materials were deposited with 7×10^{-6} torr of pressure in an Edwards Auto 500 evaporation system, using a tungsten crucible. Resistively evaporated GaAs samples were submitted to thermal annealing at 150 °C for 1h. In electrodes were submitted to thermal annealing at 150 °C for 30 min. GaAs samples were also deposited by the sputtering technique. In this case, the used substrate is SiO_2 from Korth Krinstalle, with commercial name silux5, which is cleaned in water plus detergent, followed by 3 baths in acetone under ultrasound vibration for 6 min each, followed by 3 baths in isopropyl alcohol under ultrasound vibration, again for 6 min each. Then, it is dried in pure N_2 flux. The deposition was carried out in purpose-built system [30], using 30 W of RF power, an Ar flux of 30 standard cubic centimeters per minute (sccm), and pressure of 4.5×10^{-2} torr for 60 min. The average substrate temperature during deposition was about 20 °C.

A summary of types and deposition conditions for all the samples used in this report is shown in Table 1.

2.2 Structural and morphological characterization

X-ray diffraction (XRD) data of films were obtained with a Rigaku diffractometer, model D/MAX-2100/PC, with CuK_α ($\lambda = 1.5406$ Å) radiation and scanning rate of 1°/min in the range of 20–80° (2θ), at room temperature, the procedure follows the short angle geometry for X-ray irradiation (1.5°). A current of 20 mA and a potential of 40 kV were used. Atomic force microscopy (AFM) was carried out in a Park Systems equipment, model XE7, in the mode

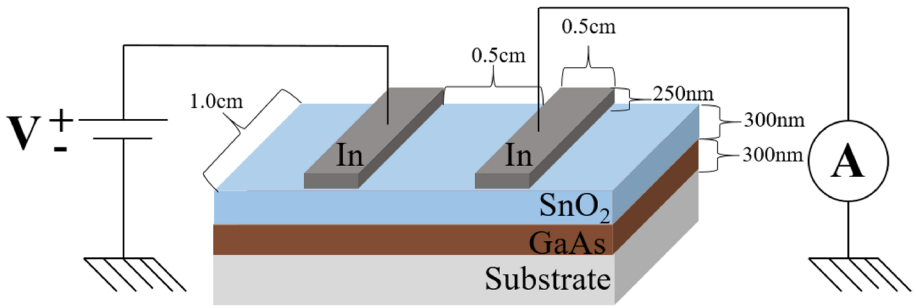

Fig. 2 Heterojunction geometry, showing the in contact on top and layout to perform electrical characterization measurements

Table 1 Identification of GaAs, SnO_2 and heterojunction samples

Sample[a]	Material	Properties
GER1	GaAs	Deposited by resistive evaporation (ER)/soda-lime glass substrate/thickness 250 nm/annealing at 150 °C/30 min
GER2	GaAs	Deposited by resistive evaporation (ER)/soda-lime glass substrate/thickness 380 nm/annealing at 150 °C/30 min
GSP1	GaAs	Deposited by sputtering (SP)/silica glass substrate/thickness 300 nm/annealing at 150 °C/30 min
S1000	SnO_2:1%Ce^{3+}	Sol–gel-dip-coating SnO_2 doped with 1%Ce^{3+}/quartz substrate/15 layers (thickness about 300 nm)/annealing at 1000ºC/1h
SG1	SnO_2:1%Ce^{3+} GaAs	Bottom: 10 layers of 1%Ce^{3+-}doped on soda-lime glass substrate/ annealed at 500ºC/1h Top: resistive evaporated GaAs/annealing 150 °C/30 min
GS1	GaAs SnO_2:1%Ce^{3+}	Bottom: GaAs deposited by sputtering/silica glass substrate Top: 10 layers of 1%Ce^{3+-}doped SnO_2 annealed at 150 °C/30 min
GS3	GaAs SnO_2:1%Ce^{3+}	Bottom: GaAs deposited by sputtering/Si (100) substrate Top: 10 layers of 1%Ce^{3+-}doped SnO_2/annealed at 150 °C/30 min
GS4	GaAs SnO_2:1%Ce^{3+}	Bottom: GaAs deposited by resistive evaporation Top: 5 layers of SnO_2/annealing 150 °C/30 min

[a]Labels S (SnO_2) and G (GaAs) indicate the deposition order

non-contact for sample deposited by resistive evaporation and contact mode for the sample deposited by sputtering.

2.3 Electrical and optical characterization

Current measurements as function of temperature were carried out under vacuum conditions, in a helium closed circuit cryostat (Janis Research), coupled with a Lake Shore Cryotronics temperature controller. The electrical signal data were collected using a Keithley electrometer, model 617. The following light sources are used to provide excitation to the electrical transport properties: (1) the fourth harmonic (266 nm) of a Nd:YAG pulsed laser, with 4.8 mJ of energy and 10 Hz of pulse frequency, (2) InGaN LED (440–460 nm) and 15 W of power, (3) He-Ne laser (628 nm) with 1.5 mW of power. (4) tungsten-halogen lamp (150 W) plus a long-pass filter, which cuts off wavelengths lower than 850 nm.

For the photoluminescence (PL) measurements in the ultraviolet to visible range, samples were excited with the 325 nm line of a He-Cd laser and the signal was detected by a GaAs photomultiplier detector cooled with liquid nitrogen. In the PL measurements, the sample temperature was controlled by using a closed cycle He cryostat. A single configuration monochromator was used for selecting the emitted signal.

3 Results and discussion

Figure 3 shows X-ray diffraction data for two heterojunction samples deposited in opposite order: sample SG1 with deposition order SnO_2/GaAs, and sample GS1, with deposition order GaAs/SnO_2. Diffractograms present the diffuse

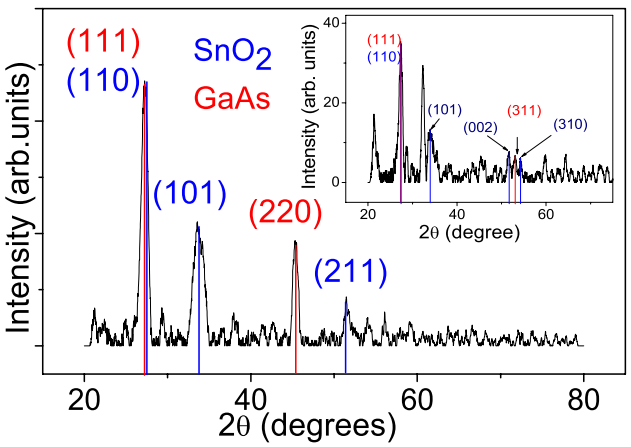

Fig. 3 X-ray diffratogram for the SnO_2/GaAs heterojunction (sample SG1). Peaks labeled with *red color* are characteristic of GaAs, while the *blue color* are from SnO_2. *Inset* X-ray diffratogram for the GaAs/SnO_2 heterojunction (sample GS1). (Color figure online)

profile typical of nano-crystallized domain. The labeled peaks correspond to the planes of tin dioxide with rutile structure (JCPDS-41-1445) and planes of GaAs (JCPDS-80-0016) [31]. Characteristic peaks of SnO_2 are seen at 33.7° and 51.5° corresponding to (101) and (211) crystallographic planes, besides planes (002) and (310), seen in the inset. Characteristic peaks of GaAs are seen at 45.4° and 53.7°, related to (220) and (311) planes. At 27.1° there is probably an overlapping of two peaks: plane (100), characteristic of SnO_2, and plane (111) of GaAs. The GaAs (220) peak is more evident (intense) for the diffractogram of SG1 sample where the GaAs layer is on top, whereas the SnO_2 peaks are more evident for the GS1 sample, with the oxide on the top, as expected. Due to the highly diffuse and noisy profile of these difractograms, a crystallite size estimation was not performed. It is important to mention the low thermal annealing temperature of the SnO_2 layer in this latter case (sample GS1), because 150 °C (Table 1) is quite low to crystallize SnO_2, but if a higher temperature was used it could degrade the GaAs layer. Then, it is easily concluded that there a great structural disorder in this sample, and one should expect very small crystallites.

Figure 4 shows AFM micrographs for GER2 and GSP1 GaAs samples. In the left side, micrographs concerns AFM for sample GER2, with a 3D image at the top picture and a 2D surface image at the bottom. These measurements were carried out in non-contact mode, due to the surface roughness, which could damage the contact. In the right side the AFM pictures are for sample GSP1, with 3D image at the top, and a 2D surface image at the bottom. In this case the system operation was in the contact mode. Figure 4 allows the comparison between these methods for the deposition of GaAs, allowing inferring on the quality of interface and SnO_2 layer grown on top of them. For the GER2, it can be seen the formation of larger agglomerates of nanoparticles, with 80 nm of average size. These agglomerates does not allow a good resolution for AFM image of sample GER2, because the pointer "jumps", making difficult the simulation of 3D topography (Fig. 4, left bottom picture). For the GSP1 sample, the micrographs evidence that the surface has smaller grains, about 20 nm of average size. The surface morphologies of films deposited by sputtering are clearly more regular than films deposited by resistive evaporation. Then, the possibility of interface conduction (2DEG-like) is clearly more probable for the GaAs/SnO_2 when the bottom layer is deposited by sputtering, due to surface smoothness.

The possible Ce^{3+} light emission from this sort of heterojunction may be verified by photoluminescence data, which were recorded for samples GS1 and GS4. Although the sputtering sample presents a better interface and also a better emission, only a small signal was recorded for the heterojunction in which the bottom layer is GaAs

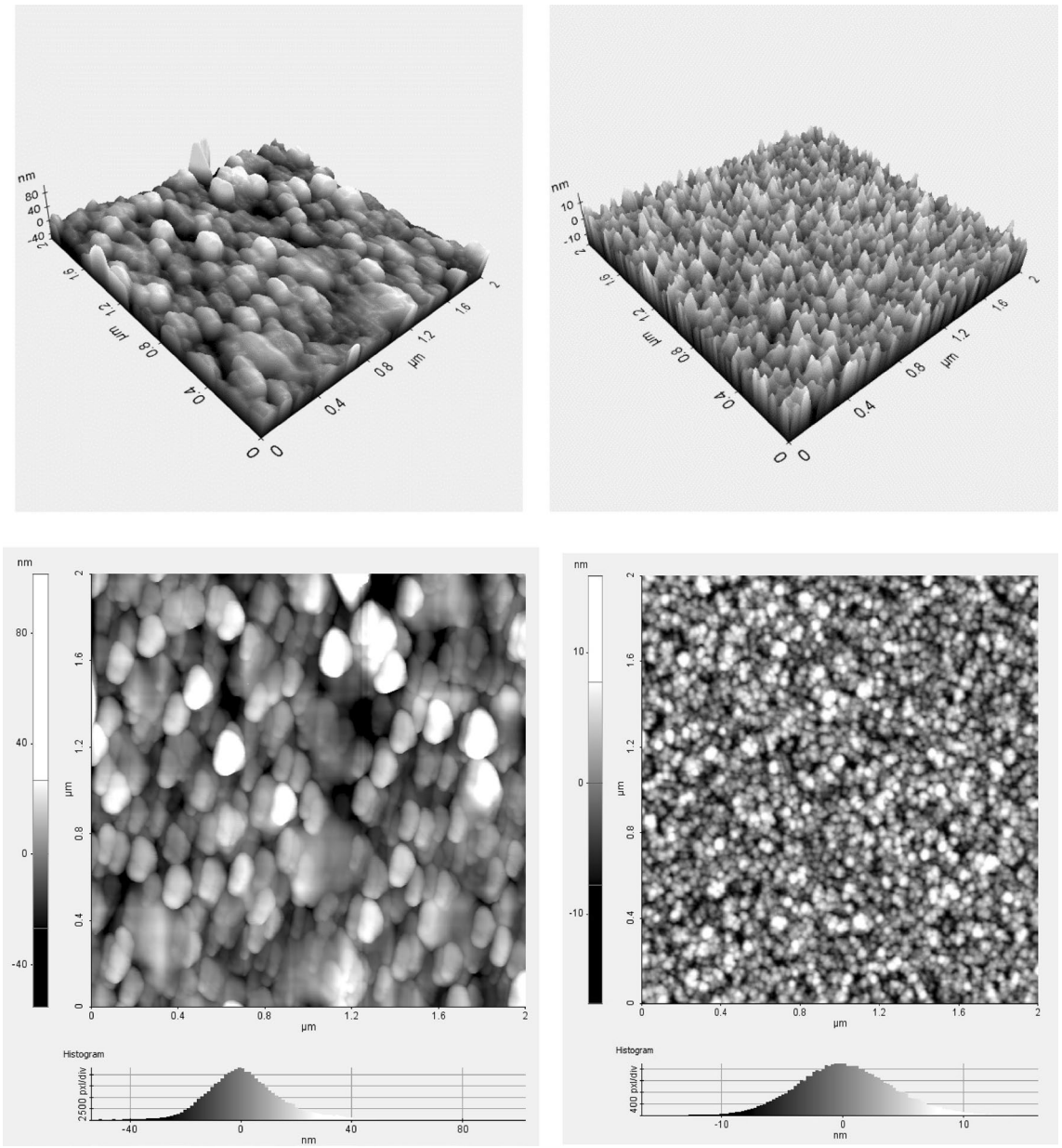

Fig. 4 (*Left*) Micrographs obtained by AFM for sample GER2, (*top*) 3D image, (*bottom*) 2D surface. (*right*) AFM for sample GSP1, (*top*) 3D image, (*bottom*) 2D surface

deposited by this technique (sample GS1). This signal is quite small and dominated by a broad band (not shown), which overcomes the Ce^{3+} emission. Then, in order to make sure that Ce^{3+} has a recordable emission when incorporated in SnO_2 films, a 1% Ce doped SnO_2 sample was deposited on quartz (sample S1000) and annealed at high temperature (1000 °C). An identically deposited sample, but where the dopant was Eu^{3+} has originated very defined emission spectra from the rare-earth ion [9]. Figure 5 shows the photoluminescence spectra for sample S1000 at different temperatures. The emission begins to become more evident about 250 K and has greater intensity at 10 K. As the temperature is reduced from room temperature, there is a more intense and defined spectrum. It is possible to observe a wide band between approximately 375 and 500 nm with a maximum around 420 nm. This peak can be associated with the cerium ion (Ce^{3+}) emission, related to transition from level 5d to 4 f level, sublevel $^2F_{5/2}$ [32, 33]. In the inset of Fig. 5 it is done a deconvolution of the PL spectra measured at 10 K, which presents higher intensity and higher definition for the whole temperature range. In this deconvolution, four

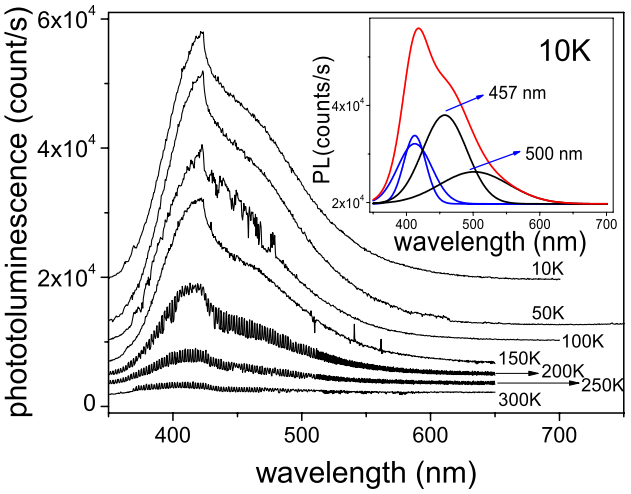

Fig. 5 Photoluminescence for sample S1000 at distinct temperatures. *Inset* deconvolution for PL at 10 K, where the *blue bands* are related Ce^{3+}, emission. *Broad band in black* are probably associated with defects in the SnO_2 matrix. (Color figure online)

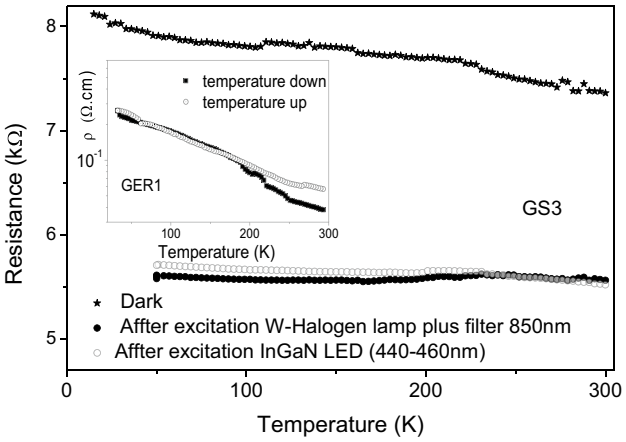

Fig. 6 Resistance as a function of temperature for heterojunction sample GS3, performed in the dark and under the effect of irradiation with different light sources: 1—InGaN LED (440–460 nm) and 2—tungsten-halogen lamp plus 850 nm long pass filter. *Inset* resistivity as function of temperature for sample GER1 (GaAs film)

bands were obtained: two bands (blue) have maximum intensity at 410 nm, value very close to Ce^{3+} emission about 420 nm, which corresponds to the Ce^{3+} transition from level 5d level to 4f ($^2F_{5/2}$) [32]. The other bands have the peak centered about 457 nm and 500 nm, and are not related to Ce^{3+} transitions.

The obtained broad band centered at 457 nm, may be attributed to deep level defect formed due to oxygen vacancies. Oxides are quite vulnerable to oxygen defects, and when doped with different size ions, in this case with Ce^{3+}, they can lead to additional negative charges. These charges are compensated by the formation of oxygen vacancies. When a hole is trapped by an oxygen vacancy, it recombines with electrons from the conduction band originating the observed emission [34, 35]. The broad band around 500 nm may be mainly associated with the presence of point defects, such as oxygen vacancies in SnO_2 nanoparticles [36]. Similar broad bands were found recently for heterojunction GaAs/SnO_2 where the oxide layer is doped with Eu^{3+} [9]. In that case, the broad band is blue shifted for increasing thermal annealing temperature as well as sample crystallite size increase. It was attributed to electron transfer from oxygen vacancies to acceptor Eu^{3+} ions, or nanocrystalline defects, originated from the disorder in the material. Considering the highly disordered condition of the SnO_2 layer in the heterojunction sample in this report, it is expected that this broad band overcome the Ce^{3+} emission. A very faint emission was obtained for the heterojunction (not shown) as mentioned earlier. A more organized condition of the GaAs bottom layer may lead to an oriented growth of the SnO_2 top layer and probably allows emission with better efficiency and then, allow signal separation.

Considering the electrical characterization, Fig. 6 shows resistance as a function of temperature for a GaAs/SnO_2 heterojunction sample and for a GaAs thin film deposited by resistive evaporation (in the inset). This figure shows an important result of the electrical characterization for the GaAs/Ce-doped SnO_2 heterojunction. For the heterojunction sample GS3, the resistance is measured on different conditions: in the dark and under the effect of irradiation with two different light sources: (1) InGaN LED (440–460 nm) and (2) tungsten-halogen lamp plus a high pass filter, which cuts off wavelengths lower than 850 nm. For these measurements, the light source was focused on the sample for six minutes at low temperature before starting the temperature raising and the collecting of electrical current data. For the data obtained in the dark, it was observed that the sample has its resistance decreased as the temperature is raised. However, when the sample is exposed to light excitation with energy below the bandgap of SnO_2 and above the bandgap of GaAs, the heterojunction resistance significantly decreases and remains constant during the measurements, even with variation of about 250 K in temperature. A possible explanation for this effect, after light excitation, is the generation of electron–hole pairs in the GaAs, with the electrons drifting to the interface region, where they remain confined, affecting the transport mechanisms. As these electrons keep trapped, there is a permanent change in electrical transport. On the other hand, the generated holes recombine with the electrons of the SnO_2 layer, located close to the interface, since there are electrons in excess in the SnO_2 layer, naturally n-type. Practically, no change is observed in electrical transport with temperature rise, because the trapped electrons at the interface quantum well are separated from scattering centers,

then the electron mobility is not influenced by temperature, besides the electron concentration at interface well remains constant, strongly suggesting a 2DEG-like behavior Then, the electrical resistivity is temperature-independent. The GaAs surface of the film deposited by sputtering is more suitable for this type of phenomena, as inferred from the AFM images, Fig. 4, which shows the smoother surface compared to deposition by resistive evaporation. Resistivity versus temperature data is shown in the inset of Fig. 6, for GaAs GER1 thin film, which was measured during the cooling down and another data series was taken during sample heating, both performed in dark conditions. It can be seen that the resistivity behavior is about the same for both conditions, temperature up and temperature down, and at 300 K the sample resistivity is about 10^{-2} Ω cm.

In order to verify the effect of both the interface 2DEG-like as well as the influence of deposition order of the heterojunction on the transport properties, measurements of current as function of applied voltage at different temperatures were performed, after the sample be submitted to different exposition to monochromatic light from distinct sources. Figure 7 shows current–voltage measurements for the heterojunction SG1 carried out in dark and under irradiation condition with different sources of light: fourth harmonic of Nd:YAG laser (266 nm), He–Ne laser (628 nm) and InGaN LED (450 nm), at 190 K. The inset in Fig. 7 shows the same type of measurement for this sample, but at 70 K. Y-axis is in log scale in order to allow better visualization of the light sources effect. Plotting the negative part of the I–V curve allows observing that sample showed an ohmic behavior for both temperatures (not shown). As regards the effect of different sources of light, the GaAs layer acts as a shield for the majority of excitation sources, preventing the sample from being excited with light irradiation. It shall be noticed that for the light source which has an energy above the SnO_2 bandgap value (Nd:YAG laser) there is no effect on the sample conductivity. However, it can be observed a slight decrease in sample conductivity for irradiation with light sources with energy above GaAs bandgap and lower than the SnO_2 bandgap. We believe that it is related to the doping with Ce^{3+}, which generates a high concentration of ions located at the grain boundary as the segregation process is very extreme. There is a tendency for the doping ion to be located at grain boundary layer and oxygen vacancies surround it as concluded for Sb-doped SnO_2 using EXAFS measurements [37]. Considering the grains located near the SnO_2/GaAs interface there is a high concentration of Ce^{3+} ions near the interface. These Ce^{3+} ions, which act as acceptors in SnO_2, can trap electrons coming from the ionization of electron–hole pairs in the GaAs layer. Again, holes recombine with the electrons in the SnO_2 layer which is naturally n-type, the overall effect is a decrease in conductivity of the sample [38].

Figure 8 shows current–voltage measurements to the heterojunction sample GS4 (which has the reverse order of deposition as compared to sample SG1, of Fig. 7), on which the GaAs bottom layer is deposited by resistive evaporation. These measurements are carried out in the dark and under the effect of different light sources, at 190 K. The light sources used are the same used for excitation of sample SG1. The inset in Fig. 8 shows the same type of measurement for this sample, but taken at 70 K. Again, the figures are in a logarithmic scale for better visualization of the irradiation effects with monochromatic light. It can be seen in Fig. 8 that for illumination with the fourth harmonic of the Nd:YAG laser, a significant increase in the current was observed. This light source has energy above the bandgap value of SnO_2 and GaAs, generating

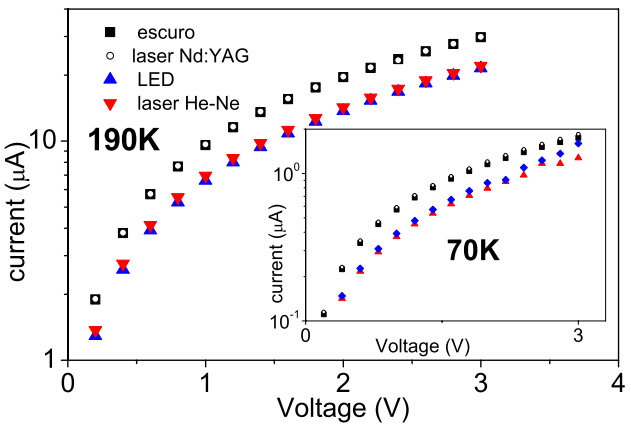

Fig. 7 Current as function of voltage for sample SG1 in the dark at 190 K, and under effect of distinct light sources: 1—fourth harmonic of Nd:YAG laser (266 nm), 2—He–Ne laser (628 nm) and 3—InGaN LED (440–460 nm). *Inset* same measurement at 70 K

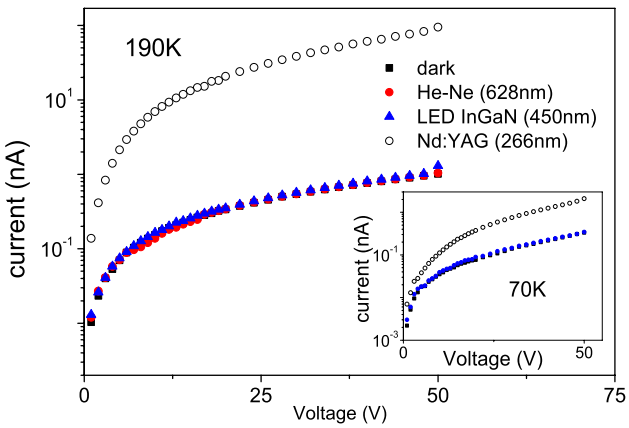

Fig. 8 Current as function voltage at 190 K, for sample GS4 in the dark, and under effect of distinct light sources: 1—fourth harmonic of Nd:YAG laser (266 nm), 2—He-Ne laser (628 nm) and 3—InGaN LED (440–460 nm). *Inset* same measurement at 70 K

high excitation of the top layer of sample GS4, compared to other light sources. Excitation with He–Ne laser and the InGaN LED have little influence on the behavior of the sample conductivity, with the measured values very close to those measured in the dark. Regardless of the measured temperature (70 and 190 K) there is a permanent effect on the sample conductivity when excited with fourth harmonic of the Nd:YAG laser, even after removing the irradiation. As mentioned earlier, the He-Ne laser and the InGaN LED had a fairly larger influence in the excitation of heterojunction samples SnO_2/GaAs, however, for the GS4 sample excitation with this light source has little influence on the current (compared to measurements in the dark). As in the sample GS4 the SnO_2 film is deposited on top of the GaAs film, this ends up being excited by the Nd:YAG laser and shows apparently a permanent change in the conductivity of the material at this low temperature. In this case, it seems that only the SnO_2 is excited because the energy of the light source is greater than its bandgap (about 3.6 eV). For light sources having energy above the bandgap of GaAs (1.42 eV for single crystal, at room temperature) and below the bandgap of the SnO_2 no significant change in the electric current was observed. This result is in opposition to what happened to sample GS3, where the bottom layer is GaAs deposited by sputtering. In that case a large increase in the conductivity and the temperature independent data lead to the hypothesis of a 2DEG-like formation at the interface, which clearly does not happen for sample GS4.

4 Conclusion

It was observed that photo-excitation of GaAs/SnO_2 heterojunction with selected irradiation sources decreases drastically its resistance. Besides, the sample exhibits an unusual behavior when the temperature is increased: the temperature variation has little influence on the resistance values, meaning that the current is practically constant. This behavior was associated with the presence of interface conduction, a two-dimensional electron gas, 2DEG-like behavior at the GaAs/SnO_2 interface.

The deposition order of the layers as well as the GaAs deposition method is fundamental to provide excitation from the 2DEG-like quantum well, which strongly contributes for the sample conductivity. When the GaAs is the bottom layer the 2DEG can be excited by light with energy below the SnO_2 bandgap and above the GaAs bandgap. Energies above the SnO_2 bandgap only excite the top oxide layer. When the GaAs is the top layer it acts as a radiation shield, and only effects from the ions close to the interface are noticed.

Efficient luminescence from the Ce^{3+} ion in the heterojunction can be obtained as the emission from the rare-earth ion can be separated from the matrix emission, because they are very close and overlap. We believe that a more organized GaAs bottom layer may contribute in this direction.

The luminescence from Ce^{3+}-doped oxides in the form of thin films provides accessibility to construction and operation of luminescent and electroluminescent devices. Besides, the possibility of temperature independent conduction of the interface opens new possibilities for application in optoelectronic devices, combining the Ce^{3+} emission with high electron mobility, making easier and faster the operation of electroluminescent devices.

Acknowledgements The authors would like to thank Prof. Andre L.J. Pereira for the help in preparing the GaAs films by sputtering, and the Brazilian agencies: CAPES, CNPq (Grant 471359/2013-0) and Grants 2006/00480-9 and 2016/12216-6 São Paulo Research Foundation (FAPESP).

References

1. M. Ishii, S. Komuro, T. Morikawa, J. Appl. Phys. **94**(6), 3823–3827 (2003)
2. S.C. Ray, M.K. Karanjai, D. Dasgupta, Surf. Coat. Technol **102**(1), 73–80 (1998)
3. E. Dien, J.M. Laurent, A. Smith, J Eur. Ceram. Soc **19**(6–7), 787–789 (1999)
4. H. Peng, H. Song, B. Chen, J. Wang, S. Lu, X. Kong, J. Zhang, J. Chem. Phys. **118**(7), 3277–3282 (2003)
5. X. Yang, M.J. Jurkovic, J.B. Heroux, W.I. Wang Appl. Phys. Lett. **75**(2),178–180 (1999).
6. S.M. Sze, *Physics of Semiconductor Devices* (Wiley, New York, 1985)
7. T. F. Pineiz, L. V.A. Scalvi, M.J. Saeki and E. A. Morais, J. Electron. Mat. **39**(8), 1170–1176 (2010).
8. T.F. Pineiz, E.A. de Morais, L.V.A. Scalvi, C.F. Bueno, Appl. Surf. Sci. **267**, 200–205 (2013)
9. C.F. Bueno, L.V.A. Scalvi, M.S. Li, M. J. Saeki, Opt. Mater. Express **5** 59–72 (2015).
10. G. Du, Y. Cui, X.C. Xia, X.P. Li, H.C. Zhu, B.L. Zhang, Y.T. Zhang, Y. Ma Y, Appl. Phys. Lett. **90**(24), 243504–243506 (2007)
11. M. Soylu, A.A. Al-Ghamdi, O.A. Al-Hartomy, F. El-Tantawyd, F. Yakuphanoglu, Physica E Low Dimens. Syst. Nanostruct. **64**, 240–245 (2014).
12. S.T. Tan, J.L. Zhao, S. Iwan, X.W. Su, X. Tang, J. Ye, M. Bosman, L.J. Tang, G.Q. Lo, K.L. Teo IEEE Trans. On Electron. Dev. **57**(1):129–233 (2010).
13. E. Cuculescu, I. Evtodiev, M. Caraman, Thin Solid Films **517**(7), 2515–2518 (2009)
14. S. Vatavu, H. Zhao, I. Caraman, P. Gasin, C. Ferekides, Thin Solid Films **519**(21), 7176–7179 (2011)
15. J.L.B Maciel Jr, E.A. Floriano, L.V.A. Scalvi, L.P. Ravaro, J Mater Sci **46**, 6627–6632 (2011)
16. M.H. Boratto, L.V.A. Scalvi, Ceram. Int. **40**, 3785–3791(2014)
17. M.H. Boratto, L.V.A. Scalvi, J.L.B. Maciel Jr, M.J. Saeki, E.A. Floriano, Mater. Res. **17**(6), 1420–1426 (2014)
18. P. Dorenbos Phys. Rev. B Condens. Matter Mater. Phys. **64**, 125117 (2001).
19. K. Annapurna, R.N. Dwivedi, P. Kundu, S. Buddhydu, Mater. Lett. **58**, 787 (2004)

20. H. Zhang, X. Fu, S. Niu, G. Sun, Q. Xin, J. Lumin. **115**, 7 (2005)
21. F. Gu, S.F. Wang, M.K. Lu, Y.X. Qi, G.J. Zhou, J. Cryst. Growth **255**, 357 (2003)
22. F. Gu, S.F. Wang, M.K. Lu, Y.X. Qi, Opt. Mater. **25**, 59 (2004)
23. Y. Yang, L. Liu, M. Li, C. Mi, Y. Liu, X. Su, J. Zhang, X. Li, F. Yu, S. Cai. Sci. Adv. Mater. **7**(7), 1304–1309 (2015)
24. Z. Mao, Y. Zhu, Y. Wang, L. Gan, J. Mater. Sci. **49**(13), 4439–4444 (2014)
25. K. Horn., in Electronic Structure of Semiconductor Surfaces, ed by K. Horn, M. Scheffler. Handbook of Surface Science, vol 2. (Elsevier, Amsterdam, 2000), p. 385–431.
26. D.C. Tsui, Phys. Rev., 24, 303–305 (1970)
27. C.W. Bark, P. Sharma, Y. Wang, S.H. Beak, S. Lee, S. Ryu, Nano Lett. **12**, 1765–1771 (2012)
28. Y. Wang, M.K. Niranjan, S.S. Jaswal, E.Y. Tsymbal, Phys. Rev. B **80**, 165130-1-10 (2009)
29. E.Y. Wang, R.N. Legge, IEEE Trans. Electron Dev. **25**(7), 800–803 (1978)
30. G.D. Azevedo, J. H. D. Silva, E. Avendano, Nucl. Instr. Methods Phys. Res. Sect. B Beam Interact. Mater. Atoms **238** (1–4), 329–333 (2005)
31. JCPDS-Joint Commitee on Powder Diffraction Standards/International Center for Diffraction Data-ICDD, Powder Diffraction Data (Pennsylvania, JCPDS/ICDD, 1983)
32. L. Bian, F. Du, S. Yang, Q. Ren, Q.L., Liu. J. Lumin. **137**, 168–172 (2013)
33. C.C. Viana, H.R. Paes Jr, Cerâmica **51** (317), 24–29 (2005).
34. M.S. Inpasalini, A. Singh, S. Mukherjee. J. Mater. Sci. Mater. Electron. **27**, 4392–4398 (2016)
35. S. L. Ko, S. Park, C.-W. Kim, D. Lee, M.-S. Choi, C. Lee, C. Jin, Appl. Phys. A **121**, 715–721 (2015)
36. R. Sánchez Zeferino, U. Pal, R. Meléndrez, M. Barboza Flores, Adv. Nano Res. **1**(4), 193–202 (2013)
37. V. Geraldo, V. Briois, L.V.A. Scalvi, J. C.V. Santilli, Eur. Ceram. Soc **27**, 4265–4268 (2007)
38. C.F. Bueno, D. H. O. Machado, T. F. Pineiz, L.V.A. Scalvi, Mater. Res. **16** (4), 831–838 (2013).